JOURNAL OF SOLID STATE CHEMISTRY 70, 185–198 (1987)

Heat Capacity of $MnAs_{0.88}P_{0.12}$ from 10 to 500 K: Thermodynamic Properties and Transitions*

ABDUL K. LABBAN AND EDGAR F. WESTRUM, JR.

Department of Chemistry, University of Michigan, Ann Arbor, Michigan 48109

AND HELMER FJELLVÅG, FREDRIK GRØNVOLD, ARNE KJEKSHUS, AND SVEIN STØLEN

Department of Chemistry, University of Oslo, Blindern, N-0315 Oslo 3, Norway

Received December 29, 1986

The heat capacity of $MnAs_{0.88}P_{0.12}$ has been measured by adiabatic shield calorimetry from 10 to 500 K. It is shown that very small energy changes are connected with two magnetic order–order transitions, indicating that these can be regarded as mainly "noncoupled" magnetic transitions. At higher temperatures contributions to the excess heat capacity arises from a magnetic order–disorder transition, a conversion from low- to high-spin state for manganese, and a MnP- to NiAs-type structural transition. The observed heat capacity is resolved into contributions from the different physical phenomena, and the character of the transitions is discussed. In particular it is substantiated that the dilational contribution, which includes magnetoelastic and magnetovolume terms as well as normal anharmonicity terms, plays a major role in $MnAs_{0.88}P_{0.12}$. The entropy of the magnetic order–disorder transition is smaller than should be expected from a complete randomization of the spins, assuming a purely magnetic transition. Thermodynamic functions have been evaluated and the respective values of C_p, $\{S_m^\circ(T) - S_m^\circ(0)\}$, and $-\{G_m^\circ(T) - H_m^\circ(0)\}/T$ at 298.15 K are 68.74, 72.09, and 32.30 J K^{-1} $mole^{-1}$, and at 500 K 56.05, 108.12, and 56.64 J K^{-1} $mole^{-1}$.

Introduction

Extensive research on the $MnAs_{1-x}P_x$ ($0.00 \leq x$ 0.18) solid-solution phase has revealed the presence of a large number of crystallographic and magnetic structures (see (*1–7*) and references therein). The present contribution concerns $MnAs_{0.88}P_{0.12}$ which is characterized by two crystallographic and four magnetic phases (*6, 7*). At low temperatures ($T < T_D = 460 \pm 10$ K) the MnP-type structure prevails, giving rise to intriguing magnetic properties. A poorly characterized modification of the double *a*-axis helimagnetic structure H_a' is found at the lowest temperatures ($T < T_{S1} = 60 \pm 10$ K). This ordering pattern transforms into a ferromagnetic structure with moments arranged along the *b*-axis, which in turn converts to a regular H_a-type helimagnetic structure at $T_{S2} = 200 \pm 10$ K. In contrast to these magnetic order–order transitions, which are somewhat sluggish, a well-defined magnetic order–disorder transition

* Dedicated to Dr. H. Nowotny.

0022-4596/87 $3.00

takes place at $T_N = 243 \pm 5$ K (*6*). The low-temperature MnP-type structure transforms continuously into a NiAs-type structure which is stable above T_D. This continuous MnP $\rightleftharpoons$ NiAs-type transition is accompanied by a low- to high-spin conversion which takes place in the entire range below T_D (*8, 9*). A more complicated phase diagram and transition pattern for $MnAs_{1-x}P_x$ than that reported in Refs. (*2, 6, 7*) is described by Govor (*10, 11*), but this discrepancy may merely reflect concentration fluctuations in the samples.

Although the different crystal and magnetic structures are reasonably well characterized, the nature of the phase transitions is less well known. The magnetic transitions may be divided into two categories, mainly pure magnetic and strongly coupled magnetoelastic transitions. The magnetic order–order and order–disorder transitions belong to the former type and are accompanied by minor changes in the crystal structure (*6, 7*). In contrast to this, the low- to high-spin conversion is strongly coupled to the continuous NiAs $\rightleftharpoons$ MnP-type crystal structure distortion (*6, 7*). The large changes in the structural parameters are ascribed to normal anharmonicity terms, magnetovolume, and magnetoelastic contributions (*12*).

In the present paper the heat capacity of $MnAs_{0.88}P_{0.12}$ from 10 to 500 K is reported for the first time. The present results are compared with the heat capacity of other $MnAs_{1-x}P_x$ compositions, as obtained by differential scanning calorimetry measurements (*7, 13, 14*). The enthalpy and entropy of the transitions are evaluated, and their nature is discussed.

Experimental

Synthesis

MnP and MnAs were synthesized from high-purity Mn flakes (99.99%), P lumps (99.999%), and As lumps (99.999%) from Koch-Light Laboratories Ltd. (England). The mixture of the elements was heated in evacuated, sealed silica-glass tubes. The temperature in the horizontally positioned furnaces was increased in steps of 30 K per 8 hr to 1173 K. After cooling the samples to room temperature during 1 day, they were carefully crushed and subjected to a further annealing at 1173 K for 1 week. Four ternary samples of $MnAs_{0.88}P_{0.12}$, each weighing about 15 g, were synthesized similarly from MnP and MnAs. After a first heat treatment at 1173 K for 5 days the samples were crushed and jointly annealed at 973 K for about ~15 weeks before being cooled to room temperature during 1 day.

Characterization

The characterization of the samples was done by powder X-ray diffraction. Room-temperature photographs were taken in an 80-mm-diameter Guinier camera, using Cu$K\alpha_1$ radiation and silicon as internal standard, a (293.15 K) = 543.1065 pm (*15*). Unit cell dimensions were derived by the method of least squares using the program CELLKANT (*16*). The resulting unit cell dimensions (a = 556.8(1) pm, b = 350.1(1) pm, and c = 620.1(2) pm) are in good agreement with previous results (*2, 6, 7*). The slight deviations between values obtained by X-ray diffraction and those obtained by neutron diffraction (*6*) are presumably caused by uncertainty in wavelength determination and sample positioning in latter experiments.

Calorimetric Technique

5 to 350 K (University of Michigan). The cryogenic measurements were made in the Mark X cryostat described previously (*17*) using intermittent heating, adiabatic equilibrium methods. The programming, data logging, and calorimetry were computerized as described elsewhere (*18*). A

gold-plated copper calorimeter (designated W-61) was loaded with 52.45 g of $MnAs_{0.88}P_{0.12}$. The buoyancy corrections are calculated for a density of 6.88 g cm^{-3}. Following evacuation, 2.2 kPa of purified helium was added to the calorimeter to enhance thermal equilibration. The calorimeter was then sealed with Cerroseal (50 Pb–50 Sn) solder. Two cylindrical OFHC copper capsules were placed within the restraining pellet vanes of the calorimeter to avoid damage to the calorimeter wall upon transitional expansion of the sample.

270 to 500 K (University of Oslo). The high-temperature calorimeter apparatus and measuring technique have been described in detail earlier (*19*). The computer-operated calorimeter was intermittently heated and surrounded by electrically heated and electronically controlled adiabatic shields. The sample was enclosed in an evacuated and sealed silica-glass tube of about 50 cm^3 in volume, tightly fitted into the silver calorimeter. Due to the extremely large thermal expansion of the sample, compressible silica cords were mixed with the sample to avoid cracking the silica-glass tube at elevated temperatures. A central well in the tube served for the heater and the platinum resistance thermometer. The mass of the sample used in the high-temperature experiments was 62.29 g.

Calibrations. The platinum-resistance thermometer for the low-temperature calorimeter was calibrated by the U.S. National Bureau of Standards, and that for the high-temperature calorimeter locally, at the ice, steam, tin, and zinc points. Temperatures are judged to correspond with IPTS 1968 to within 0.02 K from 4 to 300 K, and within 0.08 K above this temperature. All measurements of mass, resistance, potential, and time are referred to standardizations and calibrations performed at U.S. National Bureau of Standards.

The heat capacities of the empty calorimeters were determined in a separate series of experiments. The heat capacity of the empty calorimeter was 37% of the total at 10 K, 42% at 50 K, 28% above 300 K for the low-temperature measurements, and about 70% in the high-temperature measurements.

Small corrections were applied for temperature excursions of the shields from the calorimeter temperature. Further corrections were applied for differences in amounts of lead–tin solder, helium gas, and Apiezon-T grease for the low-temperature calorimeter and for differences in mass of the silica-glass containers for the high-temperature calorimeter.

Result

Heat Capacity and Thermodynamic Properties

The experimental heat capacities of $MnAs_{0.88}P_{0.12}$ for the low- and high-temperature ranges are given in chronological order in Table I and presented graphically in Fig. 1. The approximate temperature increments used in the determinations can usually be inferred from the adjacent mean temperatures in Table I. A curvature correction generally applied to the low-temperature data was not used in the transitional regions.

The estimated standard deviation of a single heat capacity measurement in the low-temperature region is about 1% from 7 to 30 K, 0.1% from 30 to 300 K, and 0.2% from 300 to 350 K. In the higher temperature region it is about 0.3%.

The experimental heat capacities for the low- and high-temperature regions were fitted to polynomials in temperature by the method of least squares. The fitting and especially the joints between the fitted segments were checked by inspection of plots of dC_p/dT against T. At the lowest temperatures the heat capacity was extrapolated

assuming a linear C_p/T versus T^2 (i.e., Debye T^3 law) relationship down to 0 K.

Values of the thermodynamic functions was obtained from the polynomial expressions by numerical integration using Simpson's rule (*20*). The evaluated data are presented in Table II for selected temperatures. The accuracy in the function values is estimated to be within 0.2% above 30 K.

The heat capacities of $MnAs_{0.89}P_{0.11}$ and $MnAs_{0.87}P_{0.13}$, as read from Figs. 5 and 6 in (*13*), are about 11% higher than the present ones at 100 K and 3% higher at 200 K. The corresponding values for $MnAs_{0.90}P_{0.10}$ at 130 and 200 K (*7*) are 1 and 3% higher than the present ones, respectively. In the intermediate temperature range no direct comparison is possible. However, above T_D fairly constant values of the heat capacity, independent of the composition (*13, 21*), have been observed. This indicates that the C_p value at 500 K for $MnAs_{0.90}P_{0.10}$ (*7*), as obtained from DSC measurements, is about 5% too high, whereas the values for $MnAs_{0.89}P_{0.11}$ and $MnAs_{0.87}P_{0.13}$ (*13*) are about 1% too high.

Resolution of the Heat Capacity

In order to obtain values for the thermodynamic functions connected with the structural and magnetic transitions, a nontransitional heat capacity was first evaluated. The observed heat capacity may, to a first approximation, be considered as composed of four main contributions: a constant volume C_V, a dilational C_d, an electronic C_e, and a magnetic C_H heat capacity. At low temperatures C_p may be approximated as

$$C_p = \beta T^3 + TV\alpha^2\kappa^{-1} + \gamma T + C_H,$$

where β and γ are constants, V is the molar volume, α is the thermal volume expansion coefficient, and κ is the isothermal compressibility. No estimates of the magnon contribution from a helimagnetic structure

TABLE I

HEAT CAPACITY OF $MnAs_{0.88}P_{0.12}$ ($M(MnAs_{0.88}P_{0.12})$ = 124.5862 g mole^{-1})

T (K)	$C_{p,m}$ (J K^{-1} mole^{-1})	T (K)	$C_{p,m}$ (J K^{-1} mole^{-1})	T (K)	$C_{p,m}$ (J K^{-1} mole^{-1})	T (K)	$C_{p,m}$ (J K^{-1} mole^{-1})
			High-temperature measurements—University of Oslo				
	Series I	417.42	64.98	453.37	66.04	337.58	81.18
271.10	65.79	425.31	64.76	455.32	66.52	340.32	82.20
279.07	66.50[a]	433.22	64.50	457.27	67.50	343.05	82.92
287.13	67.34[a]	441.15	64.84	459.20	69.28	345.79	83.14
295.13	68.40	449.09	65.24	461.15	67.86	348.53	83.12
303.06	69.92	457.02	67.80	463.12	63.26	351.27	82.72
310.91	71.50	465.02	61.40	465.12	59.98	354.01	81.94
318.67	73.88	473.19	57.12	467.15	58.32	356.77	81.08
326.16	76.70			469.19	57.42	359.54	79.84
333.57	80.24		Series III	471.24	57.10	362.33	78.44
341.00	82.58	378.83	71.66	473.30	56.66	365.13	77.02
348.39	83.44	388.43	68.88	478.46	56.40	367.96	75.70
355.80	81.62	398.13	67.04	486.72	56.16	370.80	74.42
363.28	78.22	407.93	65.82	495.02	56.02	373.65	73.22
370.87	74.76	417.78	64.92	503.36	56.04	378.95	71.28
378.57	71.66	427.68	64.70			386.71	69.12
386.32	69.54	437.61	64.42		Series IV		
394.17	67.92	443.55	64.96	299.80	69.50		
402.12	66.64	445.52	65.26	309.66	70.98		
		447.50	65.10	319.30	73.90		
	Series II	449.49	65.14	328.74	77.64		
409.55	65.66	451.43	65.52	334.83	80.16		

TABLE I—*Continued*

T (K)	$C_{p,m}$ (J K^{-1} $mole^{-1}$)	T (K)	$C_{p,m}$ (J K^{-1} $mole^{-1}$)	T (K)	$C_{p,m}$ (J K^{-1} $mole^{-1}$)	T (K)	$C_{p,m}$ (J K^{-1} $mole^{-1}$)
		Low-temperature measurements—University of Michigan					
	Series V	205.08	56.81	18.43	0.723	67.25	17.51
206.93	57.82	209.15	58.77	19.65	0.865	71.98	19.35
211.11	59.70	213.21	60.48	20.93	0.848[a]	76.73	21.13
216.38	61.70	217.29	62.20	22.28	1.197[a]	81.51	23.10
221.44	64.34	221.37	64.13	23.39	1.438	86.34	25.00
226.48	67.91	225.43	66.66	24.63	1.680	91.21	26.68
231.44	73.73	239.99	70.23[a]	25.89	1.937	96.14	28.14
236.48	73.95	255.24	65.89	27.16	2.212	101.07	29.82
241.80	68.80			28.43	2.528	106.03	31.29
247.16	67.31		Series IX	29.72	2.852	111.02	32.73
		214.44	60.89	31.18	3.259	116.01	34.23
	Series VI	218.76	62.79	32.81	3.733	121.04	35.42
126.22	33.63[a]	223.32	65.40	34.45	4.257	126.07	36.92[a]
130.32	37.69	226.57	67.81	36.23	3.933[a]	131.12	37.91
135.39	39.08	228.50	69.65				
140.45	40.32	230.38	72.04		Series XII		Series XV
145.53	41.43	232.21	74.75	27.57	2.320	211.88	60.02
150.61	42.57	233.98	78.12	29.13	2.710	216.48	61.82
155.71	43.66	235.75	75.96	30.91	3.193	221.55	64.28
160.80	44.80	237.59	71.17	32.69	3.708	236.61	70.41[a]
165.89	45.95	240.64	69.41	34.47	4.398[a]	251.83	66.65
170.99	47.13	244.86	67.79	36.26	4.623[a]	257.14	65.91
176.09	48.31			38.15	5.936[a]	262.35	65.80
181.19	49.52		Series X	40.41	6.344	267.55	65.72
186.29	50.88	233.07	76.92	42.74	7.250	272.74	65.95
191.39	52.26	233.50	77.91	45.04	8.181	277.92	66.06
196.50	53.63	233.94	79.25	47.37	9.146	283.11	66.42
201.59	55.43	234.37	78.38	49.93	10.28	288.26	67.26
206.66	57.54	234.81	77.27	52.73	11.52	293.43	67.75
				55.55	12.75	298.57	68.79
	Series VII		Series IX	58.39	13.99		
204.06	56.28	7.190	0.175[a]	61.26	15.15		Series XVI
208.54	58.42	8.585	0.150[a]			304.27	70.61
212.60	60.26	9.519	0.183		Series XIII	308.09	71.01
216.68	61.83	10.40	0.200	53.16	11.48[a]	313.24	72.44
220.75	63.85	11.28	0.233	56.27	11.93[a]	318.37	73.78
224.81	66.42	12.16	0.266	59.99	14.64	323.49	75.86
239.36	70.46	13.13	0.308	63.74	16.14	328.60	77.85
254.58	66.26	14.17	0.366	67.76	17.82	333.69	79.63
		15.20	0.441[a]			338.79	81.81
	Series VIII	16.25	0.515		Series XIV	343.34	82.85
200.68	55.01	17.30	0.607	63.25	15.91	347.52	83.20

[a] Not used in the final fitting.

is, to our knowledge, available. If one assumes that the spin-wave contribution is of minor importance at the lowest temperatures, a plot of C_p/T^2 versus T yields γ = 13.0 mJ K^{-2} $mole^{-1}$. The value is considerably higher than 4.5 mJ K^{-2} $mole^{-1}$ found for MnAs (*21*). γ is, assuming a free-electron gas, related to the density of states at the Fermi level by $\gamma = \pi^2 k_B^2 N(E_F)/3$ (*22*). Hence, the 12% substitution of P for As in MnAs greatly affects the electronic band structure of MnAs (in terms of the latter expression $N(E_F)$ increases from 4 to 12 states eV^{-1} (unit cell)$^{-1}$).

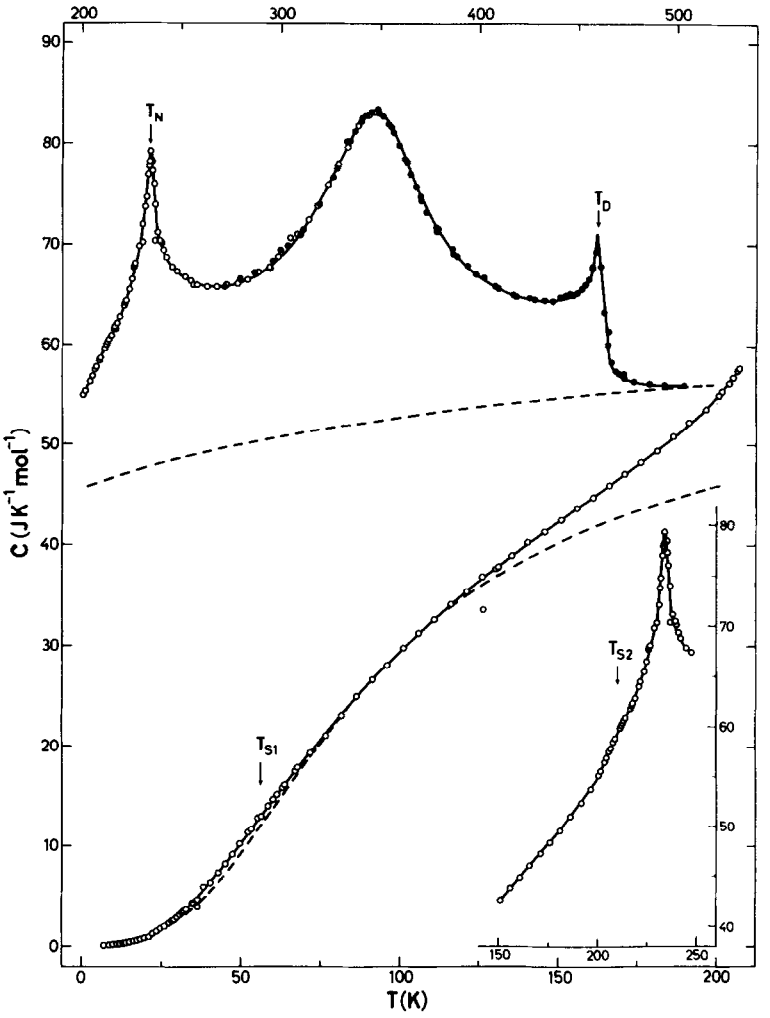

FIG. 1. Heat capacity of $MnAs_{0.88}P_{0.12}$. ○, results of University of Michigan; ●, results of University of Oslo; ---, estimated nontransitional heat capacity at constant pressure.

The lattice heat capacity is now approximated by extrapolating a constant-volume heat capacity in the harmonic approximation, using a constant Debye temperature and adding a dilational and an electronic heat capacity term. The magnetic contribution is, to begin with, neglected. The applied Debye temperature, θ_D = 364 K, was taken as the maximum value in a plot of θ_D versus temperature, whereas the electronic heat capacity was calculated by $C_e = \gamma T$, assuming that this represents a reasonable approximation even at higher temperatures. The way of deriving $C_d = TV\alpha^2\kappa^{-1}$ is, however, not obvious. The large changes in the unit cell volume, which accompany the MnP ⇌ NiAs-type transition in $MnAs_{0.88}P_{0.12}$ (*7*, *12*), give rise to a large dilational contribution (*12*). In order to calculate the nontransitional C_p curve, α, κ, and V are extrapolated from the values at low and high temperatures where the struc-

TABLE II

THERMODYNAMIC PROPERTIES OF $MnAs_{0.88}P_{0.12}$ ($M(MnAs_{0.88}P_{0.12})$ = 124.5862 g mole^{-1})

T (K)	$C_{p,m}$ (J K^{-1} mole^{-1})	$S^{\circ}_m(T) - S^{\circ}_m(0)$ (J K^{-1} mole^{-1})	$H^{\circ}_m(T) - H^{\circ}_m(0)$ (J mole^{-1})	$-\{G^{\circ}_m(T) - H^{\circ}_m(0)\}/T$ (J K^{-1} mole^{-1})
5	0.075	(0.025)	(0.091)	(0.008)
10	0.191	0.108	0.748	0.033
15	0.416	0.224	2.195	0.083
20	0.915	0.407	5.388	0.133
25	1.746	0.690	11.890	0.216
30	2.935	1.114	23.455	0.333
35	4.432	1.671	41.747	0.482
40	6.186	2.378	68.19	0.673
45	8.165	3.218	103.98	0.906
50	10.326	4.182	150.08	1.181
60	14.583	6.452	274.87	1.871
70	18.666	9.005	441.33	2.702
80	22.532	11.757	647.44	3.658
90	26.132	14.617	891.05	4.714
100	29.458	17.54	1,169.3	5.853
110	32.48	20.50	1,479.2	7.051
120	35.22	23.45	1,818.0	8.298
130	37.72	26.36	2,182.9	9.570
140	40.08	29.25	2,571.9	10.875
150	42.39	32.09	2,984.3	12.197
160	44.68	34.90	3,419.6	13.528
170	46.95	37.67	3,877.8	14.866
180	49.22	40.42	4,358.4	16.213
190	51.71	43.15	4,863.1	17.552
200	54.87	45.88	5,395.2	18.907
210	59.03	48.66	5,963.9	20.254
220	(63.10)	(51.50)	(6,575.9)	(21.609)
230	71.50	54.47	7,244.3	22.973
234.13	80.33	55.80	7,553.6	23.538
240	69.75	57.61	7,981.8	24.353
250	66.66	60.39	8,661.9	25.741
260	65.78	62.98	9,323.8	27.122
270	65.74	65.46	9,980.6	28.493
273.15	65.87	66.22	10,187.6	28.926
280	66.30	67.86	10,640.8	29.857
290	67.40	70.21	11,308.4	31.212
298.15	68.74	72.09	11,863.0	32.301
300	69.11	72.52	11,992.0	32.547
320	74.47	77.13	13,421.6	35.189
340	82.00	81.88	14,988.1	37.795
360	79.58	86.58	16,633.3	40.376
380	71.12	90.64	18,134.9	42.918
400	66.85	94.16	19,508.4	45.394
420	64.88	97.37	20,823.3	47.794
440	64.73	100.38	22,115.5	50.116
460	69.43	103.31	23,434.7	52.365
480	56.47	105.82	24,615.7	54.542
500	56.05	108.12	25,739.1	56.640

tural transition is of minor influence. The calculated nontransitional heat capacity is given by the dashed line in Fig. 1.

The present evaluation is burdened by several somewhat coarse approximations, e.g., that the free-electron-gas heat-capacity concept is assumed to be a useful representation even at higher temperatures. This is certainly only approximate since a linear dependence is to be expected only for temperatures being low with respect to the degeneracy temperature of the electron gas, $T_{deg} = E_F/k_B$. In addition changes in the electronic band structure as a function of temperature are expected to occur for phases like $MnAs_{1-x}P_x$. Also, the assumption of a constant Debye temperature is certainly approximate and θ_D probably changes when the structural MnP-type deformation takes place. In spite of this, the present evaluation is considered to be the best possible one when taking into account the current level of knowledge regarding the physical properties of such phases.

The excess heat capacity above 100 K, which includes contributions from four transitions, is given by the solid curve in Fig. 2. In the process of resolving the heat capacity into individual contributions, the large, broad peak with maximum around 347 K is regarded here as the major contribution to the excess C_p. The other contributions will be regarded as superimposed on this primary peak. Two quite different approaches for a physical interpretation of the primary peak have been proposed (*12, 13*), although both link it to the high- to low-spin conversion in $MnAs_{1-x}P_x$. The first interpretation (*13*) is based on a strongly localized picture and some aspects of this view are considered in the discussion section. The second and more recent approach interprets the primary peak in terms of a large additional dilational contribution with an origin in the coupling of the low- to high-spin conversion and the MnP $\rightleftharpoons$ NiAs-type structural transition (*12*).

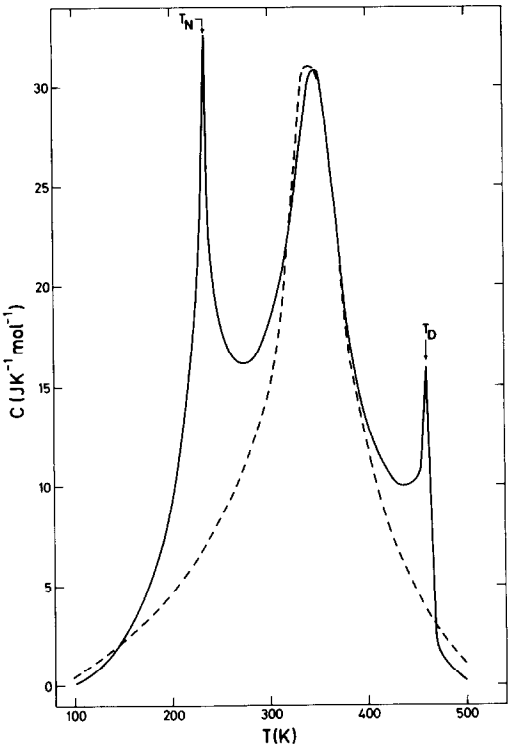

FIG. 2. Excess heat capacity. Dashed curve represents calculated dilational contribution with origin in a strongly coupled magnetostructural transition.

This phenomenologic approach does not give a microscopic picture of the spin conversion. A full account of the latter model is given in (*12*), but a short recapitulation is also included here. The dilational contribution is given by $C_d = TV\alpha^2\kappa^{-1}$. V and α are readily obtained from diffraction data (*6, 7, 12*) and the critical step is the estimation of the temperature dependence of the isothermal compressibility. In order to overcome the lack of measured compressibilities, the qualitative correspondence between chemical and external pressure (*23*), which seems obvious from the similarity of the p,T phase diagram of MnAs (*24*) and the x,T phase diagram of $MnAs_{1-x}P_x$ (*7*), is utilized. The principal effect caused by substituting P for As in MnAs is to reduce the molar volume, i.e., the same

influence as an external pressure. Consequently, proportionality between the chemical and external pressure is assumed at low substitutional levels (hence, $\kappa = V^{-1}(\partial V/\partial x)/(\partial p/\partial x)$). Assuming a temperature-independent proportionality coefficient ($\partial p/\partial x = 55$ kbar, see (*12*)), compressibilities in good keeping with the values for MnAs (*25–27*) at 295 and 450 K is obtained. The thus deduced temperature dependences of κ, α, and V are given in Fig. 3, and the resulting additional dilational contribution is given by the dashed curve in Fig. 2.

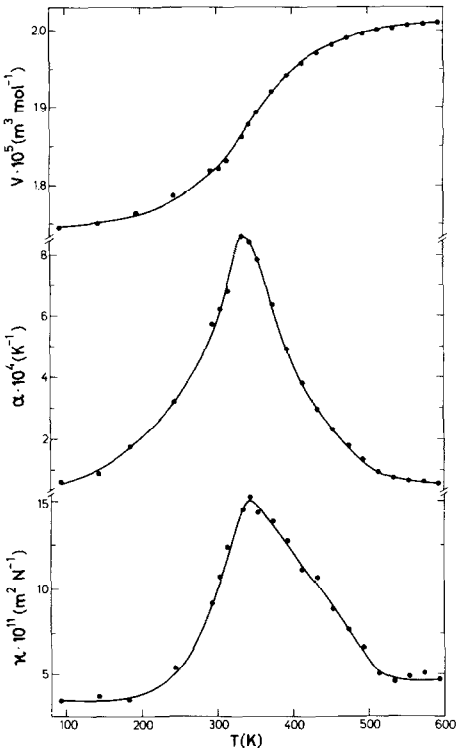

FIG. 3. Temperature dependence of molar volume, V, thermal expansion coefficient, α, and isothermal compressibility, κ.

Discussion

Magnetic Transitions

The two magnetic order–order transitions in $MnAs_{0.88}P_{0.12}$ (*6, 7*) give rise to only small effects in the heat capacity. At low temperatures the H_a' to F transition at $T_{S1} \approx 60$ K is indicated by a somewhat irregular behavior at the experimental points. The small deviation between the observed heat capacity and the calculated nontransitional $C_V + C_d + C_e$ in this temperature region of Fig. 1 does, however, most probably reflect changes in the Debye temperature, viz., lower θ_D values in this range. In contrast to this, the F to H_a transition at $T_{S2} \approx 220$ K is clearly seen as a shoulder on the dominant magnetic order–disorder peak in the inset of Fig. 1. The detailed characteristics of these transitions are, however, not known. Taking the very small and, with the present resolution, continuous changes in the structural parameters near the transition temperatures (*6, 7*) into account the contribution to the heat capacity from coupled magnetoelastic terms are probably of minor importance. Still, the minimum in the next nearest metal–metal separation within the ferromagnetic regime (*6, 7*) may indicate that the exchange interactions are related to the variation in the interatomic distances (*6*) (cf. MnAs (*28*)).

When discussing magnetic transitions, a fundamental question concerns the order of transition and it should be noted that a continuous change in the periodicity of the magnetic structures does not provide a mechanism for the order–order transitions. The magnetic moments of the H_a' and H_a structures are confined to the *bc*-plane, whereas the moment is directed along the *b*-axis in the ferromagnetic phase (*6, 7*). Hence, a first-order transition is expected if the magnetic structure determinations are fully reliable. However, physical effects which accompany first-order transitions, i.e., temperature hysteresis and discontinuous changes in crystal structure and heat capacity (see the related $Mn_{0.63}Cr_{0.37}As$ (*29*) and MnP (*30, 31*)), are not observed. This may be due to the unavoidable local varia-

tion in the composition of powdered samples, which makes the detection of very small discontinuous effects difficult. Since no definite evidence for first-order transitions is observed, a higher order transition mechanism cannot be excluded. In addition, small and continuously occurring changes in the helimagnetic structures are not easily detected by structure refinements based on powder data. For a pure magnetic transition with a simple reversal of magnetization direction for the various magnetic sublattices (without change in the magnitude of the moments) a second-order transition without change in entropy is expected (*32*). However, the anomalous behavior of the paramagnetic scattering near T_{S2} in $MnAs_{0.88}P_{0.12}$ (*9*) indicates a more complex transitional mechanism. In order to give a microscopic description of the transitions, spin waves and their mutual interaction in the vicinity of T_{S1} and T_{S2} have to be taken into account.

The magnetic order–disorder transition is observed at a somewhat lower temperature (T_N = 234.1 K) than reported in (*6*). On resolving the heat capacity as indicated in Fig. 2, the enthalpy and entropy of transition are 898 J mole^{-1} and 3.92 J K^{-1} mole^{-1}, respectively. Assuming that 1.5 spins per Mn atom becomes completely randomized above T_N the magnetic entropy should be

$$\Delta_N S = R \ln(2S + 1) \approx 7.6 \text{ J K}^{-1} \text{ mole}^{-1}.$$

This indicates a less cooperative transition, considerable short-range order above T_N, and/or associated changes in the electronic band structure. However, the likely uncertainty in the background curves (cf. Figs. 1 and 2) may hide a considerable part of the discrepancy between the deduced and calculated magnetic entropy.

No general microscopic model exists which can be applied to the magnetic order–disorder transition region. However, the magnetic heat capacity around T_N may be described in terms of power-law expressions, from which the critical exponents α' and α may in principle be deduced

$$C_H(\varepsilon) = A'/\alpha'(\varepsilon^{-\alpha'} - 1) + B' \quad \text{for } T < T_N \quad (1)$$

$$C_H(\varepsilon) = A/\alpha(\varepsilon^{-\alpha} - 1) + B \quad \text{for } T > T_N, \quad (2)$$

taking as usual $\varepsilon = (|T - T_N|)/T_N$ as the order parameter. A', A, B', and B are slowly varying functions of temperature, whereas α' and α are the critical exponents below and above T_N. The scaling hypothesis predicts that $\alpha' = \alpha$ and $B' = B$, while in general $A' \neq A$. Further terms can be included in the scaling process to cover larger ranges of ε (extended scaling). According to the universality hypothesis the critical exponents do not change as long as the dimensionality and the effective number of degrees of freedom remain unaltered. At the critical point, C_H should either diverge ($\alpha > 0$) or show a finite cusp ($\alpha < 0$). Equations (1) and (2) also incorporate the functional behavior in the exact solution of the two-dimensional Ising problem by Onsager (*33*) as a limiting case:

$$\lim[(A/\alpha)(\varepsilon^{-\alpha} - 1)] + B = -A \ln \varepsilon + B, \quad (3)$$

when $\alpha \to 0$.

On assigning a range of values to α and T_N and least-squares fitting A and B to the derived magnetic heat capacities, the following results were obtained for $\varepsilon < 0.03$, using a refined and common T_N = 234.15 K,

$$\alpha = -0.5, \quad A = 37 \text{ J K}^{-1} \text{ mole}^{-1}, \quad B = -45 \text{ J K}^{-1} \text{ mole}^{-1}$$

$$\alpha' = -0.5, \quad A' = 39 \text{ J K}^{-1} \text{ mole}^{-1}, \quad B' = -51 \text{ J K}^{-1} \text{ mole}^{-1}$$

with standard deviations 3.0 and 0.9% above and below T_N, respectively. The agreement between the observed and calculated magnetic heat capacities is shown in the lower part of Fig. 4. Results of a calculation based on the two-dimensional Ising

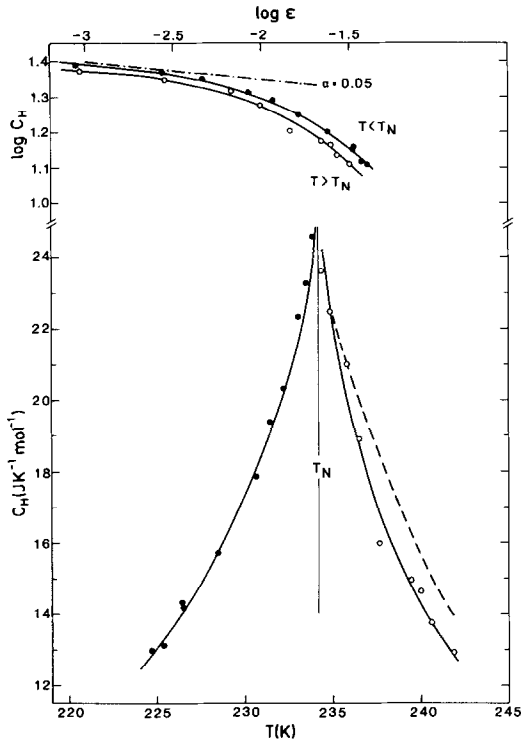

FIG. 4. Magnetic heat capacity, C_H, versus T (lower part), and log C_H versus log($|T - T_N|/T_N$) (upper part). ● and ○, experimental points; —, fits to Eqs. (1) and (2); ---, fit to Eq. (3).

model (i.e., the logarithmic singularity mentioned above) with $A' = A = 8.1$ J K^{-1} mole^{-1} and $B' = B = 2.6$ J K^{-1} mole^{-1} are also indicated (dashed curve). The calculated values for this model coincide almost completely on the low-temperature side with the solid curves from the power-law expressions, whereas the deviation on the high-temperature side in part may be ascribed to uncertainty in the chosen background level. In addition, a much better agreement would be obtained if other values of the constants were used for the high-temperature range (i.e., $A' \neq A$, $B' \neq B$). Hence, the agreement is not much better for $\alpha = -0.5$ than for α fixed to zero. This aspect is not substantiated by standard deviations, partly in view of the uncertainty in, and limited amount of, experimental data. However, the choice of data included in the critical region influences considerably the range of α's which will fit the experiments. In the upper part of Fig. 4, log C_H is plotted versus log ε and in addition a straight line corresponding to $C_H = A\varepsilon^{-\alpha}$ with $\alpha = 0.05$ is indicated. Such a straight line relationship should be expected sufficiently near T_N, where C_H is determined mainly by the exponential term. Hence, near T_N a fit with positive value of α gives the best result. The deviation of the observed C_H from a straight line for larger values of ε indicates the need for extended scaling in the range originally considered, as well as the demand for more experimental points closer to the critical temperature. However, neglecting the uncertainty in α and α', the very symmetric behavior around T_N is remarkable. This approximate symmetry, which is also evident on visual inspection of Fig. 4, is further emphasized by the finding of $\alpha = \alpha'$, $A \approx A'$, and $B \approx B'$ through the power-law analysis.

The magnetic heat capacity near the ordering temperature in MnAs and $MnAs_{1-x}P_x$ has been discussed earlier within the formalism of the mean field approximation (*14*, *34*). However, only qualitative agreement is observed due to neglect of short-range order above T_N (T_C).

Coupled Crystal Structure Transition and Magnetic Spin Conversion

Using the resolution of the heat capacity indicated in Fig. 2, the entropy and enthalpy of the large broad peak with maximums around 347 K are 12.95 J K^{-1} mole^{-1} and 4044 J mole^{-1}, respectively. This heat-capacity anomaly is connected to the occurrence of a spin conversion in $MnAs_{1-x}P_x$, as substantiated by paramagnetic scattering experiments (*8*, *9*). The continuously changing moment is intimately connected to the displacive MnP $\rightleftharpoons$ NiAs-type transition, giving rise to an

anomalous temperature dependence of the molar volume and isothermal compressibility. However, a microscopic description of the transition is not obvious, and one of the main problems concerns localization versus itineracy of the electrons. The nonintegral magnetic moment favors an itinerant model, whereas the paramagnetic moment above the Néel temperature favors a localized view.

Two microscopic models have been advanced in the interpretation of the anomaly. According to Krokoszinski *et al.* (*13*) the anomaly may be treated according to a "Bragg–Williams approximation" with high-spin Mn ions in a low-spin ensemble. Hence, starting out with a pure low-spin state at low temperatures and ending up with a pure high-spin state at high temperatures (*13*), the transition may be regarded as an order–disorder–order transition with maximum entropy when the number of high-spin ions equals the number of low-spin ions. The decrease in entropy, when the fraction of high-spin ions increases beyond one-half, must hence be stabilized by a larger decrease in enthalpy; i.e., the bonding forces must increase. The model of Krokoszinski *et al.* (*13*) implies that the overall configurational entropy equals zero. The observed entropy change consequently should depend partly on the relative degeneracy of the low- and high-spin states and partly on changes in the vibrational frequency spectrum. Since a strictly localized model is not in accord with the metallic character of $MnAs_{1-x}P_x$ (*3, 35*), the coexistence of local high- and low-spin ions in a Fermi sea was proposed (*13*) to overcome this deficiency. More recently (*14, 36*) a coupling between the structural transition and the spin conversion has been proposed as a modification of the same localized model.

In contrast to the localized model, which has an unrealistic ionic basis and spin conversion mechanism, the other microscopic approach is based on electronic band structure calculations (*37, 38*). The anomalous magnetic susceptibility and volume behaviors have been qualitatively explained on the basis of spin-fluctuation theory (*39*) which gives rise to quasi-localized moments with basis in an itinerant electron picture. In line with this, the resistivity anomaly below T_D (*40*) must be attributed to the *large* distortion of the NiAs-type structure during the progression of the MnP-type distortion.

MnP ⇌ NiAs-Type Transition

Below T_D a continuously increasing distortion of the high-temperature NiAs-type structure takes place (*6, 7*). According to Franzen *et al.* (*41*), the transition between the NiAs- and MnP-type structures can be described by three independent functions. The product of these functions is invariant for all translations of the NiAs-type structure, but not for the inversion operation. Hence, in the lack of a third-order invariant, the Gibbs energy may for small distortions, and taking coupling to strains into consideration, be formulated according to the phenomenological Landau theory (*42, 43*) as

$$G = G_0 + \tfrac{1}{2}rQ^2 + uQ^4 + eQ^2\eta + \tfrac{1}{2}E\eta^2,$$

where G_0 is the Gibbs energy of the undistorted structure, r and u are coefficients depending on the thermodynamic state of the solid, η is the strain parameter, e is the coupling factor, E is the appropriate elastic constant, and Q is the order parameter. A second-order structural transition is only possible if r passes through zero; hence assuming r has no singularity at the transition point it may be represented by an analytical function of T near T_D, i.e., $r = a(T - T_D)$. The condition for a stress-free material, $\partial G/\partial\eta = 0$, gives

$$G = G_0 + \tfrac{1}{2}a(T - T_D)Q^2 + u'Q^4,$$

where $u' = u - e^2/2E'$. $u' > 0$ specifies a

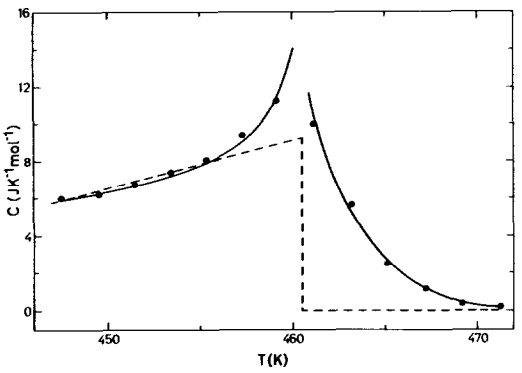

FIG. 5. Heat capacity of the MnP ⇌ NiAs-type transition in the vicinity of T_D. ●, experimental points; ---, model calculations according to Landau theory.

necessary condition for a continuous transition, and hence coupling to strain leads to an increased probability for a discontinuous transition. When the stability conditions are fulfilled, the change in heat capacity becomes $C = a^2T/8u'$ below and $C = 0$ above T_D. In Fig. 5 the experimental heat capacity is compared with the predictions of this simple version of the Landau theory. The experimental values are corrected for the background level, as extrapolated from polynomial fitting of the heat capacities in the pre- and post-transitional regions. The lack of an abrupt decrease in the heat capacity as predicted by the mean field theory, probably reflects that clusters of short-range order precede the long-range order (as $T \rightarrow T_D^+$). In order to explain such details, more subtle models taking into account the dynamic behavior of the elastic phonon instability must be used. The enthalpy and entropy of the MnP ⇌ NiAs-type transition are about 151 J $mole^{-1}$ and 0.356 J K^{-1} $mole^{-1}$, respectively. The corresponding values for the MnP ⇌ NiAs-type transitions in MnAs (*21*) and CrAs (*44*) are 25 J $mole^{-1}$ and 0.07 J K^{-1} $mole^{-1}$, and 1172 J $mole^{-1}$ and 0.92 J K^{-1} $mole^{-1}$, respectively. A common feature of these transitions is a considerably lower heat capacity on the higher temperature side of the transition. This probably reflects the occurrence of important changes in the electronic frequency distribution near T_D.

Acknowledgments

This study has been supported by the Norwegian Research Council for Science and the Humanities and by the Structural Chemistry and Chemical Thermodynamics Program, Division of Chemistry, National Science Foundation under Grant CHE-7710049.

References

1. J. B. GOODENOUGH, D. H. RIDGLEY, AND W. A. NEWMAN, *in* "Proceedings, International Conference on Magnetism," p. 542, Nottingham (1964).
2. A. ROGER AND R. FRUCHART, *Mater. Res. Bull.* **3,** 253 (1968).
3. S. HANEDA, N. KAZAMA, Y. YAMAGUCHI, AND H. WATANABE, *J. Phys. Soc. Japan* **42,** 31 (1977).
4. H. BERG AND K. BÄRNER, *J. Magn. Magn. Mater.* **4,** 69 (1977).
5. S. HANEDA, Y. YAMAGUCHI, H. WATANABE, AND N. KAZAMA, *J. Phys. Soc. Japan* **46,** 802 (1979).
6. H. FJELLVÅG, A. F. ANDRESEN, AND K. BÄRNER, *J. Magn. Magn. Mater.* **46,** 29 (1984).
7. H. FJELLVÅG, A. KJEKSHUS, AND S. STØLEN, *J. Solid State Chem.* **64,** 123 (1986).
8. L. H. SCHWARTZ, E. L. HALL, AND G. P. FELCHER, *J. Appl. Phys.* **42,** 1621 (1971).
9. A. F. ANDRESEN, H. FJELLVÅG, O. STEINSVOLL, A. KJEKSHUS, S. STØLEN, AND K. BÄRNER, *J. Magn. Magn. Mater.* **62,** 241 (1986).
10. G. A. GOVOR, *Phys. Status Solidi A* **91,** K129 (1985).
11. G. A. GOVOR, *J. Magn. Magn. Mater.* **54/56,** 1361 (1986).
12. H. FJELLVÅG, F. GRØNVOLD, A. KJEKSHUS, AND S. STØLEN, *J. Phys. C* **20,** 3005 (1987).
13. H. J. KROKOSZINSKI, C. SANTANDREA, E. GMELIN, AND K. BÄRNER, *Phys. Status Solidi B* **113,** 185 (1982).
14. K. BÄRNER AND E. GMELIN, *Phys. Status Solidi B* **132,** 431 (1985).
15. R. D. DESLATTERS AND A. HENINS, *Phys. Rev. Lett.* **31,** 972 (1973).
16. N. O. ERSSON, personal communication.
17. E. F. WESTRUM, JR., G. T., FURUKAWA, AND J. P. MCCULLOUGH, *in* "Experimental Thermodynamics" (J. P. McCullough and D. W. Scott,

Eds.), Vol. I, p. 133, Butterworths, London (1968).
18. E. F. WESTRUM, JR., *in* "Proceedings, NATO Advanced Study Institute on Thermochemistry" (R. Da Silva, Ed.), p. 745. Reidel, New York (1984).
19. F. GRØNVOLD, *Acta Chem. Scand.* **21,** 1695 (1967).
20. T. M. APOSTOL, "Calculus" Vol. II, p. 608, Wiley, New York (1969).
21. F. GRØNVOLD, S. SNILDAL, AND E. F. WESTRUM, JR., *Acta Chem. Scand.* **24,** 285 (1970).
22. C. KITTEL, "Introduction to Solid State Physics," Wiley, New York (1976).
23. A. ZIEBA, R. ZACH, H. FJELLVÅG, AND A. KJEKSHUS, *J. Phys. Chem. Solids* **48,** 79 (1987).
24. N. MENYUK, J. A. KAFALAS, K. DWIGHT, AND J. B. GOODENOUGH, *Phys. Rev.* **177,** 942 (1969).
25. N. P. GRAZHDANKINA AND A. M. BURKHANOV, *Zh. Eksper. Teor. Fiz.* **50,** 1519 (1966). [*Soviet Phys. JETP* **23,** 1013 (1966)]
26. M. DÖRFLER AND K. BÄRNER, *Phys. Status Solidi A* **17,** 141 (1973).
27. H. FJELLVÅG, H. D. HÖCHEIMER, AND W. HÖNLE, *Phys. Lett.* **118,** 293 (1986).
28. C. P. BEAN AND D. S. RODBELL, *Phys. Rev.* **126,** 104 (1962).
29. N. KOMADA, E. F. WESTRUM, JR., H. FJELLVÅG, AND A. KJEKSHUS, *J. Magn. Magn. Mater.* **65,** 37 (1987).
30. T. OKAMOTO, T. KAMGAICHI, N. IWATA, AND E. TATSUMOTO, *J. Phys. Soc. Japan* **25,** 1730 (1968).
31. Y. SHAPIRA, C. C. BECERRA, N. F. OLIVEIRA, JR., AND T. S. CHANG, *Phys. Rev.* **24,** 2780 (1981).
32. J. S. SMART, *Phys. Rev.* **90,** 55 (1953).
33. L. ONSAGER, *Phys. Rev.* **65,** 117 (1944).
34. T. KATO, K. NAGAI, AND T. AISAKA, *J. Phys. C* **16,** 3183 (1983).
35. H. BERG, K. BÄRNER, AND W. SCHRÖTER, *Phil. Mag.* **31,** 1049 (1975).
36. J. IHLEMANN AND K. BÄRNER, *J. Magn. Magn. Mater.* **46,** 40 (1984).
37. K. MOTIZUKI AND K. KATOH, *J. Phys. Soc. Japan* **53,** 735 (1984).
38. K. KATOH AND K. MOTIZUKI, *J. Phys. Soc. Japan* **53,** 3166 (1984).
39. T. MORIYA AND Y. TAKAHASHI, *J. Phys. Soc. Japan* **45,** 397 (1978).
40. K. BÄRNER AND U. NEITZEL, *Phys. Lett. A* **91,** 361 (1982).
41. H. F. FRANZEN, C. HAAS, AND F. JELLINEK, *Phys. Rev. B* **10,** 1248 (1974).
42. L. D. LANDAU AND E. M. LIFSHITZ, "Statistical Physics," Pergamon Press, London (1962).
43. A. D. BRUCE AND R. A. COWLEY, "Structural Phase Transitions," Taylor & Francis Ltd., London (1981).
44. R. BLACHNIK, G. KUDERMANN, F. GRØNVOLD, A. ALLES, B. FALK, AND E. F. WESTRUM, JR., *J. Chem. Thermodyn.* **10,** 507 (1978).